PCCP

COMMUNICATION

View Article Online
View Journal | View Issue

Cite this: *Phys. Chem. Chem. Phys.*, 2015, **17**, 23298

Received 25th June 2015,
Accepted 14th August 2015

DOI: 10.1039/c5cp03686k

www.rsc.org/pccp

Identifying the major intermediate species by combining time-resolved X-ray solution scattering and X-ray absorption spectroscopy†

Kyung Hwan Kim,[ab] Jeongho Kim,[c] Key Young Oang,[ab] Jae Hyuk Lee,‡[b] Daniel Grolimund,[d] Christopher J. Milne,[de] Thomas J. Penfold,§[d] Steven L. Johnson,[f] Andreas Galler,[g] Tae Wu Kim,[ab] Jong Goo Kim,[ab] Deokbeom Suh,[ab] Jiwon Moon,[h] Joonghan Kim,[h] Kiryong Hong,[i] Laurent Guérin,[j] Tae Kyu Kim,[i] Michael Wulff,[j] Christian Bressler[g] and Hyotcherl Ihee*[ab]

Identifying the intermediate species along a reaction pathway is a first step towards a complete understanding of the reaction mechanism, but often this task is not trivial. There has been a strong on-going debate: which of the three intermediates, the CHI_2 radical, the CHI_2–I isomer, and the CHI_2^+ ion, is the dominant intermediate species formed in the photolysis of iodoform (CHI_3)? Herein, by combining time-resolved X-ray liquidography (TRXL) and time-resolved X-ray absorption spectroscopy (TR-XAS), we present strong evidence that the CHI_2 radical is dominantly formed from the photolysis of CHI_3 in methanol at 267 nm within the available time resolution of the techniques (~20 ps for TRXL and ~100 ps for TR-XAS). The TRXL measurement, conducted using the time-slicing scheme, detected no CHI_2–I isomer within our signal-to-noise ratio, indicating that, if formed, the CHI_2–I isomer must be a minor intermediate. The TR-XAS transient spectra measured at the iodine L_1 and L_3 edges support the same conclusion. The present work demonstrates that the application of these two complementary time-resolved X-ray methods to the same system can provide a detailed understanding of the reaction mechanism.

A chemical reaction is the transformation of reactants to products and often involves many short-lived intermediate species. Identification of such species is a first (but not trivial) step towards understanding the mechanism of the reaction. Various time-resolved techniques have been developed to monitor the dynamics of reacting molecules, but different techniques may deliver conflicting answers. Time-resolved optical spectroscopies are routinely used for studying the dynamics of chemical reactions.[1–8] Optical spectroscopy is highly sensitive to particular states or chemical species of interest. Therefore, time-resolved optical spectroscopy is very powerful for detecting the fate of transient species irrespective of their abundance, but it gives only limited information on the molecular structure. In contrast, time-resolved X-ray liquidography (TRXL) and X-ray absorption spectroscopy (TR-XAS), which make use of X-ray pulses instead of optical laser pulses as a probe, are directly sensitive to changes in the molecular structure. TR-XAS can selectively measure the information on electronic and geometrical configurations around the target atom, and is thus suited for studying the interaction between, *e.g.*, a central metal atom and surrounding ligands in transition metal complexes[9–12] as well as the structural change near an absorbing atom in proteins.[13–15] In contrast, since the scattering signal comes from every atom in the sample (including the solvent), TRXL can be applied to study the reaction dynamics of small molecules containing heavy scatterers[16–20] as well as global structural changes of proteins.[21–24] Both TRXL and TR-XAS suffer from relatively low cross sections, and thus a high X-ray photon flux and/or samples of high concentration are required to compensate. However, each tool is useful for

[a] *Center for Nanomaterials and Chemical Reactions, Institute for Basic Science (IBS), Daejeon 305-701, Republic of Korea. E-mail: hyotcherl.ihee@kaist.ac.kr; Fax: +82-42-350-2810; Tel: +82-42-350-2884*
[b] *Department of Chemistry, KAIST, Daejeon 305-701, Republic of Korea*
[c] *Department of Chemistry, Inha University, Incheon 402-751, Republic of Korea*
[d] *Swiss Light Source, Paul Scherrer Institut, 5232 Villigen, Switzerland*
[e] *Laboratoire de Spectroscopie Ultrarapide, ISIC, EPFL, 1015 Lausanne, Switzerland*
[f] *Institute for Quantum Electronics, ETH Zurich, 8093 Zurich, Switzerland*
[g] *European XFEL GmbH, Albert Einstein Ring 19, 22 607 Hamburg, Germany*
[h] *Department of Chemistry, The Catholic University of Korea Bucheon, 420-743, Republic of Korea*
[i] *Department of Chemistry, Pusan National University, Busan 609-735, Republic of Korea*
[j] *European Synchrotron Radiation Facility, BP 220, Grenoble Cedex 38043, France*

† Electronic supplementary information (ESI) available. See DOI: 10.1039/c5cp03686k

‡ Present address: Ultrafast X-ray Science Laboratory, Lawrence Berkeley National Laboratory, Berkeley, CA 94720, USA.
§ Present address: Department of Chemistry, Newcastle University, Newcastle upon Tyne, NE1 7RU, UK.

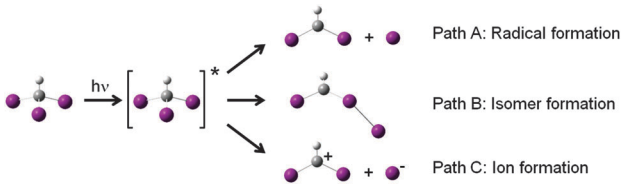

Scheme 1 Various candidate reaction pathways.

assessing the structural properties towards elucidating global reaction pathways. A comparative study of a reaction using these two complementary X-ray methods can yield more convincing results and better insight into the reaction details, but such studies have been rare so far.

The photodissociation of iodoform (CHI_3) in methanol is an interesting system due to the ambiguity about the major intermediate species (Scheme 1).[4–7,25,26] A previous study using TRXL[25] reported that the formation of a CHI_2 radical is the major reaction channel and the formation of a CHI_2–I isomer or a CHI_2^+ ion was not detected. In contrast, a subsequent laser spectroscopic study[26] reported that the isomer is formed in a few picoseconds (ps) and dissociates into CHI_2^+ and I^- ions in ~700 ps. To resolve this conflict, here we used both TR-XAS and TRXL to measure the sub-nanosecond kinetics. By comparing the results obtained by these two complementary methods, we expect a more convincing conclusion on the identity of the major intermediate species on the time scale of 0.05–2 nanoseconds (ns).

The TRXL data were measured at the ID09B beamline of the European Synchrotron Radiation Facility, following an experimental protocol described in the ESI.† Briefly, a solution of iodoform dissolved in methanol at the concentration of 1–20 mM was circulated through the sapphire nozzle. A ~2 ps laser pulse with a 267 nm center wavelength was used to initiate the photodissociation of the sample, and a time-delayed ~100 ps X-ray pulse was used to monitor the progress of the reaction. To extract the transient signal, the difference scattering curves, $\Delta S(q,t)$, were obtained by subtracting the scattering curve measured at −5 ns from the scattering curves at positive delays. To probe early events occurring within the X-ray pulse width (~100 ps), the laser-time-slicing scheme was employed (see ESI†). In the laser-time-slicing scheme, by deconvoluting the instrument response function from the scattering curves measured at time delays earlier than the time resolution, we can achieve the effective time resolution of ~20 ps and extract the dynamics occurring earlier than 100 ps.[27]

Fig. 1a shows one-dimensional difference scattering curves at four different time delays: −20 ps, 100 ps, 300 ps, and 1 ns. The scattering curve measured at −20 ps time delay was scaled up to compensate for partial contribution of the X-ray pulse to the transient signal. The four scattering patterns are identical to each other within the noise level, indicating that the major intermediate species are generated within our time resolution and stay up to 1 ns without any further change in the molecular structure. The temporal change of the peak intensity at q = 2.205 Å^{-1}, displayed in Fig. 1b, gives a clear view of the kinetics on the sub-nanosecond time scale. The rise of the signal is well

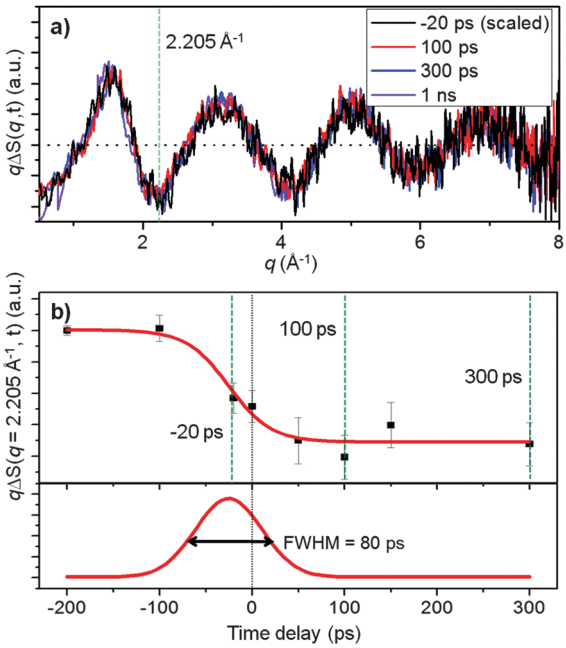

Fig. 1 Time-resolved X-ray scattering measurements of the iodoform photolysis. (a) Difference scattering curves, $q\Delta S(q,t)$, at four different time delays; −20 ps (black, scaled), 100 ps (red), 300 ps (blue), and 1 ns (violet). (b) The temporal change in the intensity at a negative peak position (q = 2.205 Å^{-1}, marked with a green dashed line in (a)) is displayed from −200 ps to 300 ps. The three time points, at which the difference scattering curves shown in (a) were measured, are indicated with green vertical dashed lines. The signal change in this time range is well described by a single error function with a width of 80 ps FWHM (bottom panel).

described by a single error function with a width of 80 ps full-width-half-maximum (FWHM), which corresponds to the instrument response function (IRF) of the ID09B beamline. Based on the constant shape of the scattering patterns at different time delays and the time trace well explained by the IRF alone, we conclude that there is no signature of further chemical reaction occurring on the sub-nanosecond time scale. This conclusion is in contrast to the result from the previous transient absorption measurement,[26] which identified the dissociation of the CHI_2–I isomer with an ~700 ps time constant, and suggests that the isomer is not the major intermediate formed in the photolysis of iodoform.

To identify the major intermediate species formed on the sub-nanosecond time scale, which is the point of controversy, the difference scattering curve at −20 ps was analyzed. Using the Debye equation, the theoretical difference scattering curves were calculated for three candidate reaction pathways (CHI_2 + I, CHI_2–I, and $CHI_2^+ + I^-$) as shown in Fig. 2. The molecular structures calculated by density functional theory were used to calculate the solute contribution. Solvent hydrodynamics and the contribution from solute–solvent interaction were also considered. The details of the theoretical analysis are described in the ESI.† In Fig. 2, the experimental curve at −20 ps and the theoretical curve are compared for each candidate pathway. It is clearly seen that the CHI_2 + I channel fits the experimental curve much better than the CHI_2–I isomer channel or the $CHI_2^+ + I^-$

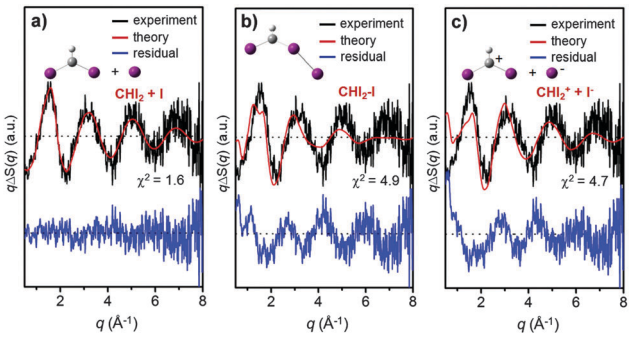

Fig. 2 Theoretical difference scattering curves at −20 ps time delay for three candidate reaction pathways: (a) dissociation into the CHI_2 radical and I, (b) CHI_2–I isomer formation and (c) dissociation into CHI_2^+ and I^- ions. Experimental (black) and theoretical (red) curves are compared at the top and the residual (blue) obtained by subtracting the two curves is displayed at the bottom.

channel, giving a substantially smaller χ^2 value (1.6) than the others (4.9 and 4.7, respectively). The difference in fit quality between the three reaction channels can be explained in terms of the contributions of solute, cage, and solvent as shown in Fig. S2 in the ESI.† The solute and cage terms of the CHI_2–I isomer channel have very different shapes from those of the CHI_2 + I channel because the CHI_2–I isomer has an additional I–I bond compared with CHI_2. The $CHI_2^+ + I^-$ channel gives a much larger cage term than other channels and therefore it yields a poor fit to the experimental curve, especially in a low q-region, despite the structural similarity of CHI_2 and CHI_2^+. We also fitted the experimental scattering curve with a linear combination of theoretical scattering curves for the three reaction pathways and found that the contributions of the CHI_2–I isomer channel and the $CHI_2^+ + I^-$ channel converge to zero within the error range. In addition to the optimized isomer structure, which has a C–I–I angle of 113° and an I–I distance of 3.174 Å, we also examined the various possible structures of the isomer with the C–I–I angle varying from 133° to 93° and the I–I distance varying from 3.674 to 2.674 Å. However, none of them fit our experimental data as well as the fit in Fig. 2b (Fig. S3 in the ESI†). This result shows that the CHI_2 radical, rather than the isomer or the CHI_2^+ ion, is the major intermediate in the iodoform photolysis. The estimated yield of the CHI_2 radical was ~8%, which is similar to the value obtained from our previous study.[25] We note that the TRXL measurement should be equally sensitive to the structure of the CHI_2 radical and the CHI_2–I isomer because X-rays scatter from every atom in the molecules.

In contrast to optical spectroscopy that can readily probe even very dilute samples, TRXL and TR-XAS require rather high sample concentrations. To check for any concentration dependence,[28] we also measured the TRXL signal of a more diluted sample (1 mM). While the difference scattering curve from the diluted sample is noisier (due to much lower signal intensity), we can confirm that the scattering curves measured from the concentrated and diluted samples have the shapes identical to each other within their noise levels (see Fig. S4 in the ESI†) and thus have the same reaction intermediates (see Fig. S6 in the ESI†). This indicates that, regardless of the sample concentration, the CHI_2 radical is the major intermediate.

The TR-XAS measurement was performed at the microXAS beamline of the Swiss Light Source at the Paul Scherrer Institute, following a typical experimental protocol[29,30] as described in the ESI.† Briefly, a ~150 fs laser pulse at 267 nm was used to dissociate CHI_3, and a tunable monochromatic X-ray pulse of ~100 ps duration subsequently probed the X-ray absorption in the transmission mode. The TR-XAS data were measured around both iodine L_1 and L_3 edges, which correspond to the formation of a core hole in the I 2s and I $2p_{3/2}$ orbitals, respectively. The absorption spectra near the L_1 edge of iodine show an additional absorption feature at the energy right below the absorption edge, which corresponds – in the atomic picture – to the 2s → 5p transition in iodine.[29,30] This feature is very sensitive to the chemical state of iodine and can be used for identifying chemical species.[29,30]

Fig. 3a shows the difference XANES spectra measured around the iodine L_1 edge at three different time delays: 100 ps, 300 ps and 1 ns. The most distinct feature peaked at 5.1857 keV, and is located at a lower energy than the main edge and thus corresponds to the 2s → 5p transition. The peak positions, amplitudes and shapes of the three transient spectra are almost identical to each other within the noise level, likely indicating that the major intermediate species are generated within the first 100 ps and remain constant up to 1 ns. To examine the kinetics on the sub-nanosecond time scale, we performed a time scan at a peak

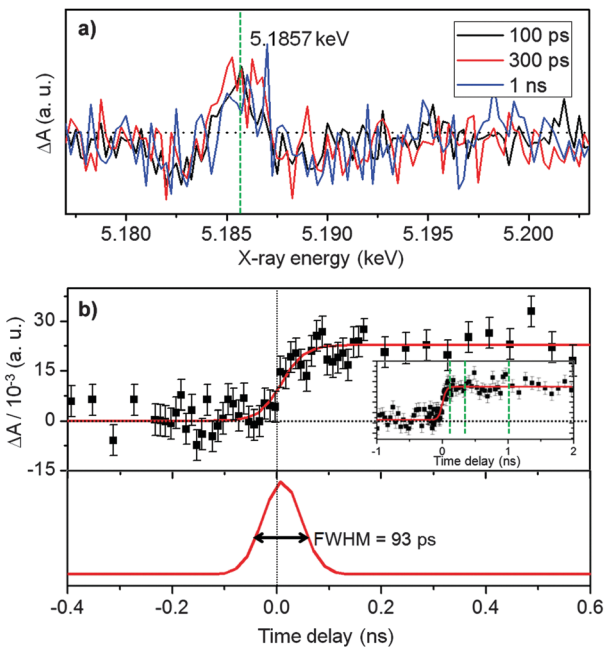

Fig. 3 The TR-XAS measurement of iodoform photolysis at the L_1 edge of the iodine atom. (a) Difference XANES spectra measured at the time delays of 100 ps, 300 ps, and 1 ns. (b) The temporal change in the difference absorption intensity at a peak position (E = 5.1857 keV) marked with a green dashed line in (a) is displayed from −0.4 to 0.6 ns. The time trace in this time range is well explained by a single error function with a width of 93 ps FWHM (red). Inset shows a longer time range up to 2 ns.

position (E = 5.1857 keV) of the difference XANES spectrum by changing the time delay between laser and X-ray pulses from −1 to 2 ns. As shown in Fig. 3b, the rise of the time trace is governed by a single error function with a width of 93 ps FWHM, which is equivalent to the IRF of the microXAS beamline, while no other kinetic component was identified.

This observation was confirmed by measuring the transient absorption spectra near the L_3 edge of iodine (see Fig. S7 in the ESI†). As for the spectra at the L_1 edge, the peak positions, amplitudes and shapes of the transient L_3-edge spectra measured at 100 ps and 2 ns are almost identical to each other within the noise level. Also, the time trace at the energy of a negative peak (E = 4.5623 keV) exhibits the same dynamics as observed in Fig. 3b, thus excluding any additional kinetics on the 0–2 ns time scale.

To identify the major intermediate species formed on subnanosecond time scale, the difference absorption spectrum measured at the L_1 edge and 100 ps was analyzed. First, we performed a fitting analysis by using static spectra of iodine-containing analogue species obtained from previous TR-XAS studies as a basis set. In particular, we used the static XANES spectra of I_2 and CHI_3 to represent the spectral features of ···I–I and ···C–I groups, respectively. For free I species, we used the static spectrum of a neutral I atom produced from the photo-induced reaction of I^- into I.[30] To generate theoretical difference XANES spectra from these static spectra, we considered (1) the depletion of the ···C–I group and the formation of the free I species for the CHI_2 + I channel and (2) the depletion of the ···C–I group and the formation of the ···I–I group for the CHI_2–I isomer channel. The quantum yield of photoproduct formation was used as a free fitting parameter for both reaction channels to adjust the overall amplitude of the theoretical difference XANES spectrum. Although neither of the fits are perfect especially for the negative feature around 5.1825 keV, probably due to the limitation of the analysis using the analogue species, we clearly see that the CHI_2 + I channel fits the experimental curve much better than the CHI_2–I isomer channel (see Fig. 4b). Secondly, we simulated theoretical absorption spectra that correspond to the 2s → 5p transition using time-dependent density functional theory (TDDFT).[31] To incorporate the effect of the solvent, the simulated spectra were generated from 100 MD configurations with 30 surrounding solvent molecules as described in the ESI.† As can be seen from the simulated absorption spectra in Fig. S8 of the ESI,† the absorption peak of the I radical is located at the same energy (5.1857 keV) as the main positive peak in our experimental difference absorption spectrum while the absorption peaks of the CHI_2–I isomer and the CHI_2^+ ion are located at higher energies by ∼4 eV than the main positive peak. Therefore, the experimental difference absorption spectrum is better explained by the formation of the I radical in the CHI_2 + I channel.

The CHI_2–I isomer, the major intermediate found by Raman and optical spectroscopy measurements,[26] was not detected, within the current signal-to-noise ratio, by either TRXL or TR-XAS measurements. Instead, the CHI_2 radical was found to be the major intermediate. A possible explanation for this discrepancy is that the

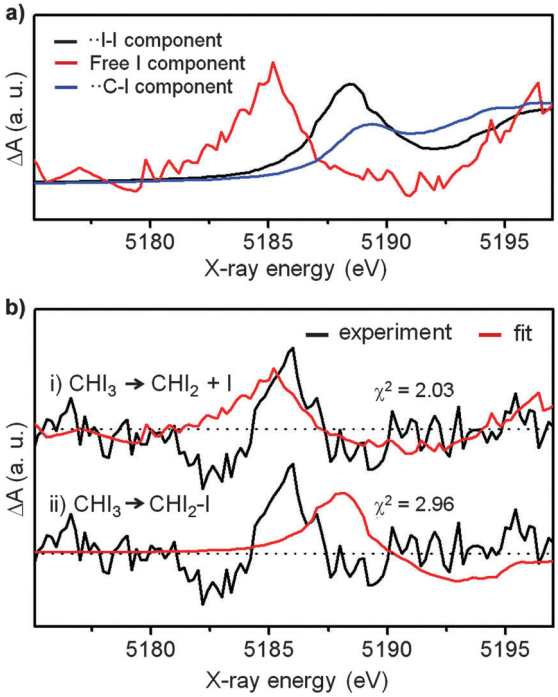

Fig. 4 (a) Static XANES spectra of various iodine-containing species measured at the L_1 edge of the iodine atom. These spectra were used as a basis for the fitting analysis shown in (b). (b) The fitting analysis of the L_1-edge difference XANES spectrum measured at 100 ps for two candidate reaction pathways: (i) CHI_2 radical + I and (ii) CHI_2–I isomer formation. Experimental (black) and theoretical (red) difference XANES spectra are compared with each other.

CHI_2–I isomer might have a much higher oscillator strength than the CHI_2 radical in the spectral window investigated in the previous study, resulting in a transient signal dominated by the response from the CHI_2–I isomer. To check this possibility, we calculated the transition energies and oscillator strengths of the excited states as well as the resonance Raman frequencies for the CHI_2–I isomer and the CHI_2 radical in various solvents including methanol (see the ESI† for details). Indeed, the CHI_2–I isomer has considerably higher oscillator strengths than the CHI_2 radical for both absorption and Raman scattering (see Tables S2 and S3 in the ESI†), irrespective of the solvent.[4] In contrast, the X-ray-based methods used in the present work are more sensitive to the global structure of the reacting molecules and thus equally sensitive to both the CHI_2 radical and CHI_2–I isomer species. Thus, the missing signature of the CH_2–I isomer in the TRXL and TR-XAS measurements suggests that the yield of the isomer might be too low to be detected by TRXL or TR-XAS.

Conclusions

In this work, TRXL and TR-XAS measurements were performed to identify the reaction intermediates of iodoform photolysis. Both methods confirm that the major intermediate is the CHI_2 radical, which is formed within the available time resolution of the techniques (∼20 ps for TRXL and ∼100 ps for TR-XAS).

In contrast, any evidence for the formation of the CHI_2–I isomer was not observed within the current signal-to-noise ratio. The identical results obtained from these two complimentary tools increase the fidelity of our conclusion, which gives an insight into the identity of reaction intermediates of the iodoform photolysis.

Acknowledgements

We thank Prof. Shunsuke Nozawa and Prof. Shin-ichi Adachi for helpful discussions. This work was supported by IBS-R004-G2. This work was supported by Basic Science Research Program through the National Research Foundation of Korea (NRF) funded by the Ministry of Science, ICT & Future Planning (NRF-2014R1A1A1002511). This research has been supported by the TJ Park Science Fellowship of POSCO TJ Park Foundation.

Notes and references

1 A. H. Zewail, *Angew. Chem., Int. Ed.*, 2001, **40**, 4371–4375.
2 P. Kukura, D. W. McCamant, S. Yoon, D. B. Wandschneider and R. A. Mathies, *Science*, 2005, **310**, 1006–1009.
3 H. Lee, Y. C. Cheng and G. R. Fleming, *Science*, 2007, **316**, 1462–1465.
4 X. M. Zheng and D. L. Phillips, *Chem. Phys. Lett.*, 2000, **324**, 175–182.
5 M. Wall, A. N. Tarnovsky, T. Pascher, V. Sundstrom and E. Akesson, *J. Phys. Chem. A*, 2003, **107**, 211–217.
6 Y. L. Li, D. M. Chen, D. Q. Wang and D. L. Phillips, *J. Org. Chem.*, 2002, **67**, 4228–4235.
7 A. N. Tarnovsky, I. Pascher and T. Pascher, *J. Phys. Chem. A*, 2007, **111**, 11814–11817.
8 A. N. Tarnovsky, V. Sundstrom, E. Akesson and T. Pascher, *J. Phys. Chem. A*, 2004, **108**, 237–249.
9 C. Bressler, C. Milne, V. T. Pham, A. ElNahhas, R. M. van der Veen, W. Gawelda, S. Johnson, P. Beaud, D. Grolimund, M. Kaiser, C. N. Borca, G. Ingold, R. Abela and M. Chergui, *Science*, 2009, **323**, 489–492.
10 L. X. Chen, W. J. H. Jager, G. Jennings, D. J. Gosztola, A. Munkholm and J. P. Hessler, *Science*, 2001, **292**, 262–264.
11 S. Nozawa, T. Sato, M. Chollet, K. Ichiyanagi, A. Tomita, H. Fujii, S. Adachi and S. Koshihara, *J. Am. Chem. Soc.*, 2010, **132**, 61–63.
12 N. Huse, H. Cho, K. Hong, L. Jamula, F. M. F. de Groot, T. K. Kim, J. K. McCusker and R. W. Schoenlein, *J. Phys. Chem. Lett.*, 2011, **2**, 880–884.
13 D. M. Mills, A. Lewis, A. Harootunian, J. Huang and B. Smith, *Science*, 1984, **223**, 811–813.
14 S. Della Longa, A. Arcovito, M. Benfatto, A. Congiu-Castellano, M. Girasole, J. L. Hazemann and A. Lo Bosco, *Biophys. J.*, 2003, **85**, 549–558.
15 A. Arcovito, C. Ardiccioni, M. Cianci, P. D'Angelo, B. Vallone and S. Della Longa, *J. Phys. Chem. B*, 2010, **114**, 13223–13231.
16 H. Ihee, M. Lorenc, T. K. Kim, Q. Y. Kong, M. Cammarata, J. H. Lee, S. Bratos and M. Wulff, *Science*, 2005, **309**, 1223–1227.
17 J. Davidsson, J. Poulsen, M. Cammarata, P. Georgiou, R. Wouts, G. Katona, F. Jacobson, A. Plech, M. Wulff, G. Nyman and R. Neutze, *Phys. Rev. Lett.*, 2005, **94**, 245503.
18 M. Christensen, K. Haldrup, K. Bechgaard, R. Feidenhans'l, Q. Y. Kong, M. Cammarata, M. Lo Russo, M. Wulff, N. Harrit and M. M. Nielsen, *J. Am. Chem. Soc.*, 2009, **131**, 502–508.
19 K. H. Kim, J. H. Lee, J. Kim, S. Nozawa, T. Sato, A. Tomita, K. Ichiyanagi, H. Ki, J. Kim, S. Adachi and H. Ihee, *Phys. Rev. Lett.*, 2013, **110**, 165505.
20 K. H. Kim, J. G. Kim, S. Nozawa, T. Sato, K. Y. Oang, T. Kim, H. Ki, J. Jo, S. Park, C. Song, T. Sato, K. Ogawa, T. Togashi, K. Tono, M. Yabashi, T. Ishikawa, J. Kim, R. Ryoo, J. Kim, H. Ihee and S.-i. Adachi, *Nature*, 2015, **518**, 385–389.
21 M. Cammarata, M. Levantino, F. Schotte, P. A. Anfinrud, F. Ewald, J. Choi, A. Cupane, M. Wulff and H. Ihee, *Nat. Methods*, 2008, **5**, 881–886.
22 H. S. Cho, N. Dashdorj, F. Schotte, T. Graber, R. Henning and P. Anfinrud, *Proc. Natl. Acad. Sci. U. S. A.*, 2010, **107**, 7281–7286.
23 S. Ibrahimkutty, J. Kim, M. Cammarata, F. Ewald, J. Choi, H. Ihee and A. Plech, *ACS Nano*, 2011, **5**, 3788–3794.
24 K. H. Kim, S. Muniyappan, K. Y. Oang, J. G. Kim, S. Nozawa, T. Sato, S. Y. Koshihara, R. Henning, I. Kosheleva, H. Ki, Y. Kim, T. W. Kim, J. Kim, S. Adachi and H. Ihee, *J. Am. Chem. Soc.*, 2012, **134**, 7001–7008.
25 J. H. Lee, J. Kim, M. Cammarata, Q. Kong, K. H. Kim, J. Choi, T. K. Kim, M. Wulff and H. Ihee, *Angew. Chem., Int. Ed.*, 2008, **47**, 1047–1050.
26 P. Z. El-Khoury, W. M. Kwok, X. Guan, C. Ma, D. L. Phillips and A. N. Tarnovsky, *ChemPhysChem*, 2009, **10**, 1895–1900.
27 J. H. Lee, M. Wulff, S. Bratos, J. Petersen, L. Guerin, J. C. Leicknam, M. Carnmarata, Q. Kong, J. Kim, K. B. Moller and H. Ihee, *J. Am. Chem. Soc.*, 2013, **135**, 3255–3261.
28 C. Y. Zhao, X. F. Lin, W. M. Kwok, X. G. Guan, Y. Du, D. Q. Wang, K. F. Hung and D. L. Phillips, *Chem. – Eur. J.*, 2005, **11**, 1093–1108.
29 C. Bressler, R. Abela and M. Chergui, *Z. Kristallogr.*, 2008, **223**, 307–321.
30 V. T. Pham, T. J. Penfold, R. M. van der Veen, F. Lima, A. El Nahhas, S. L. Johnson, P. Beaud, R. Abela, C. Bressler, I. Tavernelli, C. J. Milne and M. Chergui, *J. Am. Chem. Soc.*, 2011, **133**, 12740–12748.
31 S. D. George, T. Petrenko and F. Neese, *Inorg. Chim. Acta*, 2008, **361**, 965–972.

